Scaling for state-selective charge exchange due to collisions of multicharged ions with hydrogen

2015 J. Phys. B: At. Mol. Opt. Phys. 48 235201

(http://iopscience.iop.org/0953-4075/48/23/235201)

IOP Publishing Journal of Physics B: Atomic, Molecular and Optical Physics
J. Phys. B: At. Mol. Opt. Phys. **48** (2015) 235201 (10pp) doi:10.1088/0953-4075/48/23/235201

Scaling for state-selective charge exchange due to collisions of multicharged ions with hydrogen

A Jorge[1], Clara Illescas[1], J E Miraglia[2] and M S Gravielle[2]

[1] Laboratorio Asociado al CIEMAT de Física Atómica y Molecular en Plasmas de Fusión. Departamento de Química, módulo 13, Universidad Autónoma de Madrid, Cantoblanco E-28049 Madrid, Spain
[2] Instituto de Astronomía y Física del Espacio (IAFE, CONICET-UBA) Casilla de Correo 67, Sucursal 28, (C1428EGA) Buenos Aires, Argentina

E-mail: alba.jorge@uam.es

Received 13 April 2015, revised 1 August 2015
Accepted for publication 1 September 2015
Published 6 October 2015

Abstract

In this article we evaluate state-resolved charge exchange cross sections for Be^{4+}, B^{5+}, C^{6+}, N^{7+}, and O^{8+} projectiles colliding with atomic hydrogen employing two different methods: the classical trajectory Monte Carlo and the eikonal impulse approximations. These cross sections are used to extend previously derived scaling laws for *n*-, *nl*-, and *nlm*-distributions to highly excited final levels with $4 \leqslant n \leqslant 9$, covering energies in the range $50 - 2000$ keV/ amu. Present total and partial capture cross sections are in agreement with available experimental and theoretical data for these collision systems. Besides, the proposed scaling rules are also verified by other theories, becoming a useful instrument for plasma research.

Keywords: electron capture, scaling, multicharged ions, hydrogen, partial charge-exchange cross sections

(Some figures may appear in colour only in the online journal)

1. Introduction

Charge exchange (CX) in collisions of multiply charged ions with hydrogen atoms has attracted renewed attention in the last years. Such an interest is motivated by the importance of this process, also called electron capture, in both laboratory and astrophysical plasma environments [1]. In the case of laboratory magnetic confined plasmas, the CX between multicharged ions and neutral H plays an important role to estimate the temperature of the plasma and the density and charge of ionic impurities [2, 3], while in astrophysical plasmas it was found to be responsible for x-ray emission from comets due to the scattering of solar wind ions with cometary neutral gases, having been also detected in the heliosphere and in planetary atmospheres [4–6].

When multiply charged ions collide with H(1*s*) at intermediate and moderated high impact energies, electrons are mainly transferred to excited states of the ion, which then decay via photon emission giving rise to specific emission lines. These emission spectra, extensively employed as a diagnostic tool in plasmas [7], strongly depend on the *nl*-distribution of transferred electrons [8, 9], making the state-selective electron capture cross section a key magnitude for the analysis of the experimental data. However, partial CX cross sections into different *nl*-sublevels are less studied than their corresponding total and partial *n* values and consequently, several plasma studies assume approximated *l*-distributions for the different levels [10–12]. In this article we focus precisely on these state-selective CX cross sections, extending previously derived scaling laws for *n*-, *nl*-, and *nlm*-distributions [13] to deal with final capture levels up to the $n = 9$ shell.

Two different theoretical methods are employed: the classical trajectory Monte Carlo (CTMC) method and the eikonal impulse (EI) approximation. Each of these methods can be applied in a different region of impact energies. The CTMC method is a classical theory that results appropriate for impact velocities *v* in the range $v \sim 1 - 3$ a.u. [14], while the

EI approach is a high-energy method, which can be extended to describe CX in the intermediate velocity range as well, i.e. for velocities $v \gtrsim 2$ a.u. [13]. We use both approaches to evaluate state-selective CX cross sections for different ion-H collisions with the aim of providing reliable scaling rules that cover a wide range of incidence energies, from intermediate to high impact velocities. Notice that for highly charged ions colliding with H(1s), many scaling rules for total capture, and even for partial capture to a given n shell, have been proposed [15–18]. But for nl-distributions the studies on scaling laws are scarce [13, 19, 20]. Therefore, present state-selective scaling rules are useful tools to estimate partial contributions coming from specific final capture states, avoiding tedious calculations, specially for capture to highly excited levels.

In this article, the CTMC and EI methods are applied to evaluate CX cross sections for different bare ions—Be^{4+}, B^{5+}, C^{6+}, N^{7+}, and O^{8+}-impinging on neutral hydrogen in its ground state. The range of considered projectiles is of interest in fusion and astrophysical research. Most of these ions are found as impurities in laboratory fusion plasmas, like beryllium and carbon that are expected to be present in ITER [21, 22], or nitrogen that is routinely introduced in the ASDEX tokamak to protect the plasma-facing components [23, 24]. Also in astrophysics, ions of carbon and oxygen are considered the predominant sources of soft x-ray emission in collisions involving the solar wind [4, 25, 26].

This article is organized as follows. The theoretical methods used in this work to investigate scaling rules for partial CX distributions are presented in section 2. In section 2.1 we summarize the parametric dependence of the CX cross section to a specific final state, obtained within the EI approximation, which is here employed to derive scaling laws for highly excited final states. While in section 2.2 we show how total capture cross sections derived within the CTMC and EI approximations merge in the intermediate velocity regime, allowing us to combine both theories to produce a join CTMC-EI approach that provides reliable results for a wide range of impact velocities, from 1 a.u to 6 a.u. Scaling rules for the corresponding partial cross sections are investigated in section 3, where scaled n-, nl- and nlm-distributions are presented and discussed in sections 3.1, 3.2 and 3.3, respectively. Finally, in section 4 we outline our conclusions. Atomic units (a.u.) are used unless otherwise stated.

2. Description of the theoretical methods

2.1. Parametric dependence of the EI capture cross section to a given final state

The prior version of the EI approximation is a distorted wave method that makes use of the exact impulse wave function to describe the final collision channel, while the initial channel is represented by means of the eikonal wave function [27]. It has been successfully applied to describe CX in asymmetric collisions, where the nuclear charge of one of the particles is larger than the other, at high and intermediate impact velocities. In particular, the prior EI approach was found

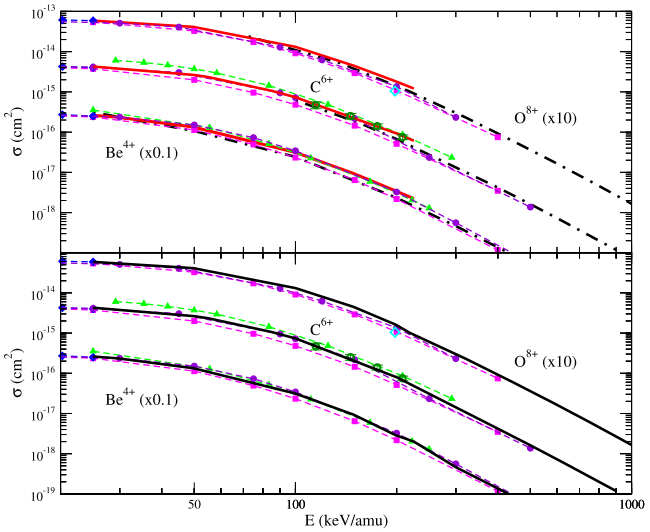

Figure 1. Total electron capture cross sections for Be^{4+}, C^{6+} and O^{8+} ions impinging on H(1 s), as a function of the incidence energy. (a) (upper panel) Calculations derived with :---, EI; ___, CTMC approachs. (b) (lower panel): — , join CTMC-EI method; other theories: ■ – –■ AOCC [32], ♦ – –♦ MOCC [33], ▲ – –▲ FBA [34], ● – –● AOCC [35]; expt.: ○ [18] and ◇ [36].

to provide proper electron capture predictions for both, multicharged ions colliding with light atoms (H and He) [13] and proton-atom collisions [28].

Following previous articles [13, 19], we use the prior EI approach to derive a scaling rule for the asymmetric reaction:

$$A^{Z_P+} + H(1s) \rightarrow H^+ + A^{(Z_P-1)+}(n, l, m), \tag{1}$$

where the charge of the fully stripped projectile, Z_P, is larger than the one of the target nucleus, Z_T (with $Z_T = 1$ for H), and n, l, m are the quantum numbers of the final electronic state, $\phi_{n,l,m}$, bounded to the projectile with final electronic energy $\varepsilon_{n,l}$. For this reaction the EI transition matrix reads [28]:

$$T^{(EI)}_{n,l,m} = \int \frac{d\vec{q}}{(2\pi)^{3/2}} \phi^*_{n,l,m}\left(\vec{q}\right) L_T^{D-*}\left(\vec{q},\ \vec{W_P} - \vec{v}\right) \times \left\{ \left(\frac{q^2}{2} - \varepsilon_{n,l} \right) I_P^{E+}\left(-\vec{v},\ \vec{W_P} - \vec{q}\right) + J_P^{E+}\left(-\vec{v},\ \vec{W_P} - \vec{q}\right) \right\}, \tag{2}$$

where $\vec{v}$ is the impact velocity and $\vec{W_P} = \vec{K_i} - \mu_P \vec{K_f}$ is the projectile momentum transfer, with $\vec{K_i}$ ($\vec{K_f}$) the initial (final) momentum of the projectile and μ_P its final reduced mass. The functions L_T^{D-}, I_P^{E+}, and J_P^{E+} represent the Nordsieck-type integrals defined in [28], and $\phi_{n,l,m}(\vec{q})$ is the Fourier transform of the final electronic wave function. From equation (2), using the explicit expressions of the L_T^{D-}, I_P^{E+}, and J_P^{E+} functions, the EI capture cross section into the n, l, m state, σ^{EI}_{nlm}, is found to satisfy [13]

$$\sigma^{EI}_{nlm} \simeq \tilde{z}_P^{-7} \left| C\left(Z_P/v\right) \right|^2 \tilde{\sigma}_{nlm}\left(\tilde{v},\ \tilde{W}\right), \tag{3}$$

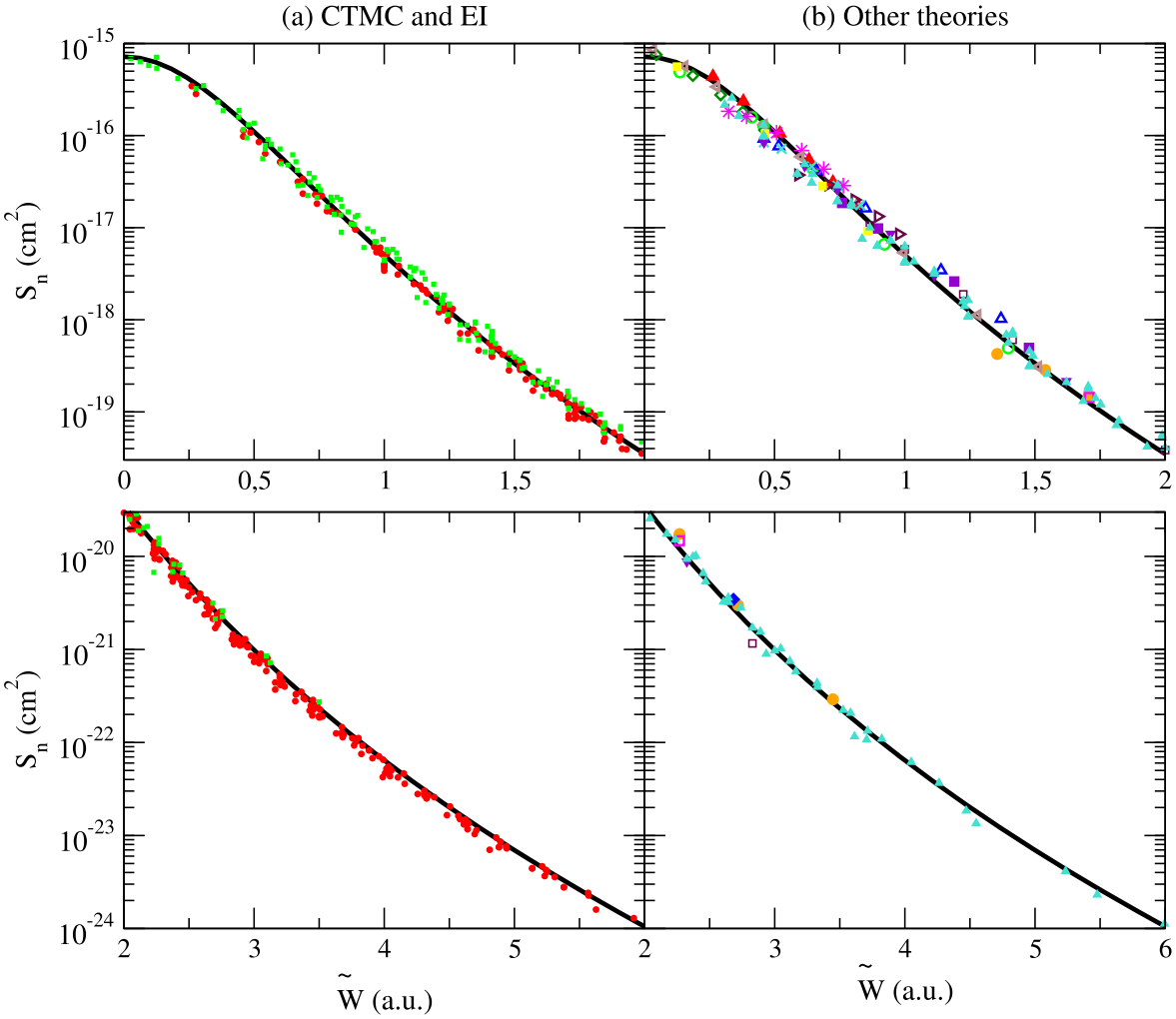

Figure 2. Scaled cross sections S_n, as a function of the scaled momentum $\tilde{W}$, for different n values in the range $n = 4 - 9$. Solid black line, proposed curve given by equation (8). Column (a) (left pannels), results for $Z_P = 4$–8 derived within the considered approaches: ● EI, ■ CTMC, each of them in the corresponding velocity range, as indicated in the text. Column (b) (right pannels), results from other theories: ●, ○ and ■ AOCC for $Z_P = 4, 6, 8$, $n = 6, 4, 7$, respectively [35]; □ and ♦ CTMC for $Z_P = 4$, $n = 6, 7$ [38]; ◊ and ▲ CDW for $Z_P = 6$, $n = 3, 4$ [39]; △ FBA for $Z_P = 6$, $n = 5$ [34]; ×, ✳ and ▷ CTMC for $Z_P = 6$, $n = 5$ and $Z_P = 8$, $n = 6, 7$ [40]; □, ▼, ◀; ■ AOCC for $Z_P = 5, 6, 7, 8$ and $n = 5, 5, 4, 3$ [41] and recommended ADAS sets for $Z_P = 6$, $n = 4, 8$ ▲ [42].

where $\tilde{z}_P = Z_P/n$ represents the mean value of the final electron velocity and

$$C(a) = \exp(\pi a/2)\Gamma(1 - ia) \tag{4}$$

is the projectile-electron Coulomb factor coming from the asymptotic conditions, with Γ the gamma function. In equation (3) the function $\tilde{\sigma}_{nlm}$ depends on the scaled parameters $\tilde{v}$ and $\tilde{W}$, denoted with tilde, which are defined as $\tilde{v} = v/\tilde{z}_P$ and

$$\tilde{W} = \frac{W}{\tilde{z}_P} = \frac{\tilde{v}^2 + \tilde{z}_T^2 - 1}{2\tilde{v}}, \tag{5}$$

respectively, with $W = \overrightarrow{W_P}.\,\overrightarrow{v}/v$ the component of $\overrightarrow{W_P}$ parallel to the incidence velocity and $\tilde{z}_T = Z_T/\tilde{z}_P$ ($\tilde{z}_T = \tilde{z}_P^{-1}$ for H targets).

For positive $\tilde{W}$ values, the function $\tilde{\sigma}_{nlm}$ of equation (3) presents a weak dependence on $\tilde{v}$ and consequently, it can be approximated by an universal function of $\tilde{W}$, depending only of the final quantum numbers n, l, m; that is,

$$\tilde{\sigma}_{nlm}\left(\tilde{v},\, \tilde{W}\right) \approx u_{nlm}\left(\tilde{W}\right). \tag{6}$$

In this article we will use this approximation, together with equation (3), to derive state-selective scaling laws for capture to highly excited levels, with main quantum numbers in the range $4 \leqslant n \leqslant 9$. As stated in [13], the approximated relation of equation (6) starts to fail for impact velocities lower than 2 a.u. when the condition $\tilde{z}_P > 1$ is not verified.

2.2. Join CTMC-EI approach: total capture cross sections

In this section we inspect the validity of the used theoretical approaches—CTMC and EI—by comparing total capture cross sections for the studied collision systems with available experimental data and with results obtained from other theories.

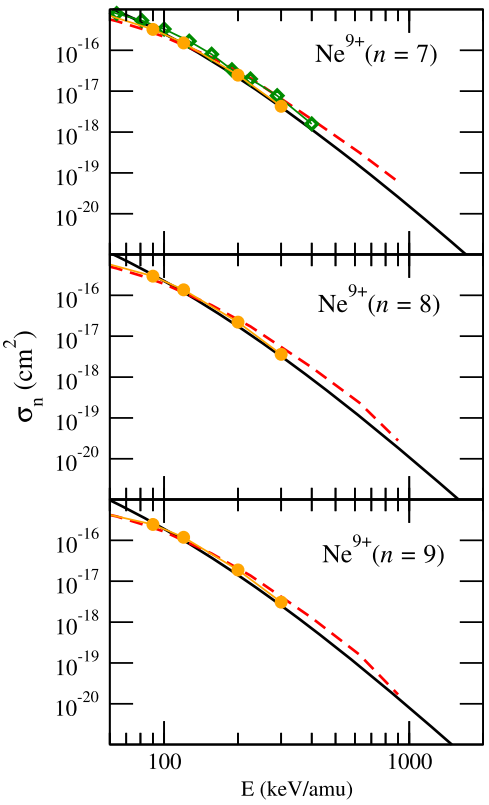

Figure 3. Partial CX cross sections σ_n, as a function of the impact energy, for Ne^{10+} + H(1 s) collisions. Solid black line, present scaling; calculations: -- CTMC [44], ◇ one-electron-diatomic-molecule (OEDM) [44], ● AOCC [35].

The present CTMC calculations were computed using a superposition of ten standard microcanonical distributions, fitting the radial probability density of the atomic hydrogen [29]. Nuclear straight-line trajectories and a statistic of 2×10^5 electrons have been considered. The trajectories have been integrated up to $t_{max} = 500v^{-1}$. Notice that capture to low n levels ($n \lesssim 3$) is well characterized by the usual microcanonical distribution, but for higher n levels, like those considered in this article, the hydrogenic density-fitted one provides a better description of the electron capture process [30, 31].

Concerning the EI approach, each electron capture cross section to a given n, l, m state was calculated separately, involving a three-dimensional integral on the momentum space, as given by equation (2), and a further integration on the final angular distribution of the scattered projectiles. For highly excited final levels, such numerical calculations were almost prohibitive twenty years ago, forcing us to use extrapolation rules [13], but now they can be done in a reasonable CPU time (for example, for the state (n, l, m) = (9, 8, 0) of carbon, it takes less than 3' in a PC I7 computer). In this article we evaluated EI total capture results by adding (n, l, m)- cross sections up the shell $n = 9$, while the contribution of final levels with $n \geqslant 10$ was estimated by using an extrapolation rule based on the n-dependence of the Brinkman-Kramer cross section, as given by equation (12) of [13].

In figure 1(a) we display CTMC and EI total CX cross sections for Be^{4+}, C^{6+}, and O^{8+} colliding with H(1s), as a function of the impact energy, considering a different velocity range for each method: $v \leqslant 3$ a.u. for the CTMC method and $v \geqslant 2$ a.u. for the EI one. For the three projectiles, the CTMC and EI curves fairly agree each other in the intermediate energy region, between 100 and 200 keV amu^{-1}, and in the case of beryllium, the accord also extend to lower energies. In order to quantify the level of concordance of both theories, we can mention that for C^{6+} projectiles the differences between CTMC and EI total capture cross sections at 100 keV amu^{-1} are around 15%, increasing up to 27% at 200 keV amu^{-1}. This fact allows us to combine both theoretical methods by merging them around 100 keV amu^{-1} to build a join CTMC-EI approach, which provides realistic cross sections in a wide velocity region, ranging from intermediate to high incidence velocities.

Total cross sections derived within the join CTMC-EI method are shown in figure 1(b) and compared with results obtained from other theories and with available experimental data. For all the projectiles the curve corresponding to the join CTMC- EI approximation is in good accord with values derived from different theories, like semiclassical close-coupling approaches with molecular (MOCC) [33] or atomic (AOCC) [32, 35] wave functions, or the first born approximation (FBA) [34. Join CTMC-EI results are also in agreement with available experimental data for carbon and oxygen projectiles in the intermediate energy regime [18, 36]. Such a concordance is an indication of the adequate description of the CX process obtained by means of the merge of the CTMC and the EI methods.

The same criterion is followed in the next section to combine the CTMC and EI theories also at the level of state-selective cross sections, where the differences between CTMC and EI n-resolved cross sections at 100 keV amu^{-1} are 20% at most for Be^{4+} projectiles, decreasing up to a relative error lower than 10% as Z_P augments. At low velocities, the join CTMC-EI results verified that the most populated n-level, n_{max}, qualitatively agrees with the $Z_P^{3/4}$ scaling law [37], but the value of n_{max} slowly decreases as the velocity increases, tending in all the cases to the ground level at very high velocities.

3. Results

3.1. Scaling law for partial n-resolved cross sections with n ⩾ 4

In this section we focus on the partial CX cross section into a given final n level, σ_n, which is defined as $\sigma_n = \sum_{lm} \sigma_{nlm}$. From equations (3) and (6) we obtain the following approximated relation for σ_n:

$$S_n = \frac{\tilde{z}_P^7 \sigma_n}{\left|C\left(Z_P/v\right)\right|^2} \simeq U_n\left(\tilde{W}\right) \simeq \sum_{lm} u_{nlm}\left(\tilde{W}\right), \qquad (7)$$

where U_n is expected to be an universal function of $\tilde{W}$, depending on the main quantum number n. In previous articles [13, 19], this scaling rule was successfully tested for

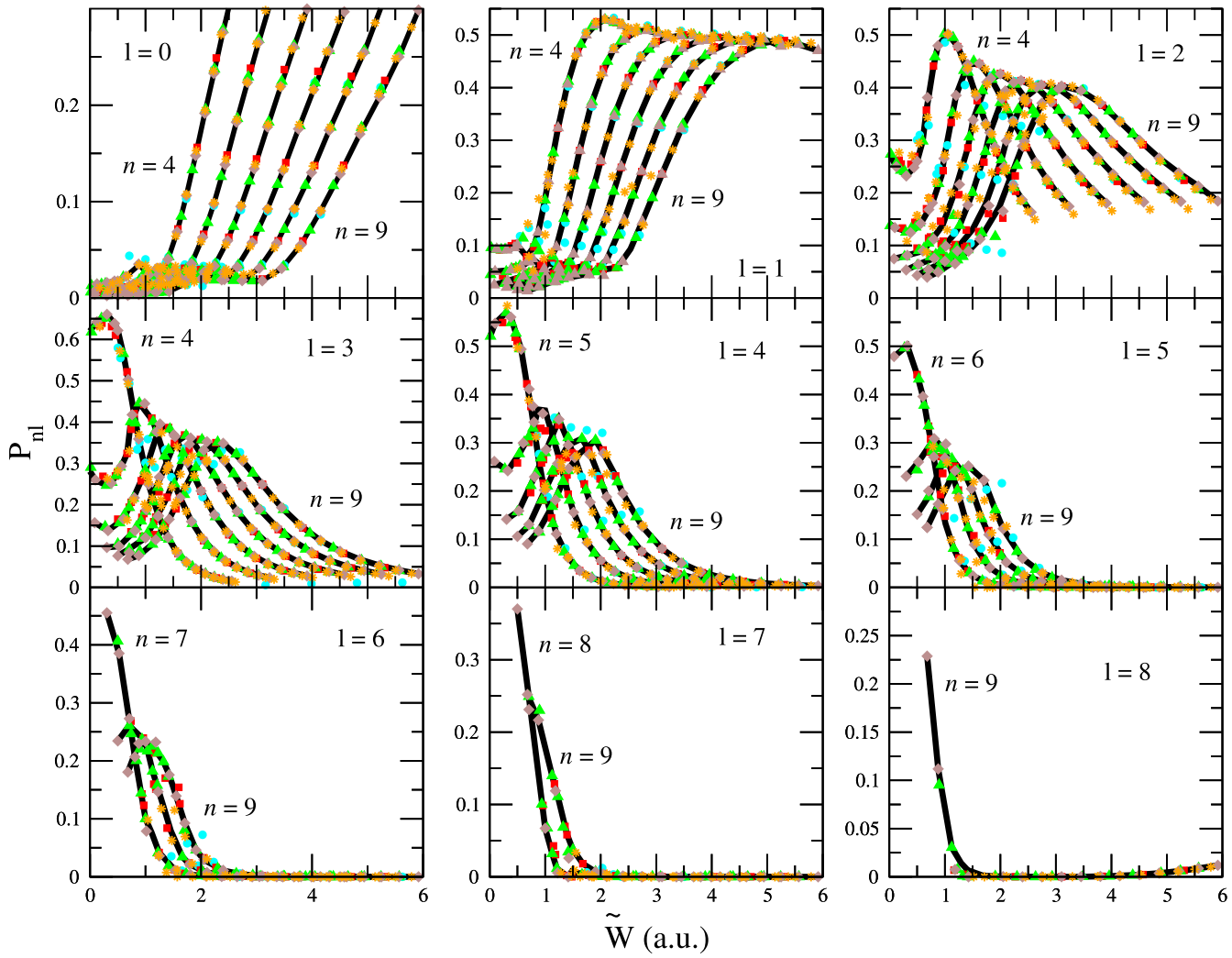

Figure 4. Join CTMC-EI P_{nl} distributions as a function of $\tilde{W}$. Solid black line, present scaling, given by equation (9); results for different projectiles: ● Be^{4+}, ✳ B^{5+}, ■ C^{6+}, ▲ N^{7+}, ♦ O^{8+}. In each panel the curves shift from left to right as n increases.

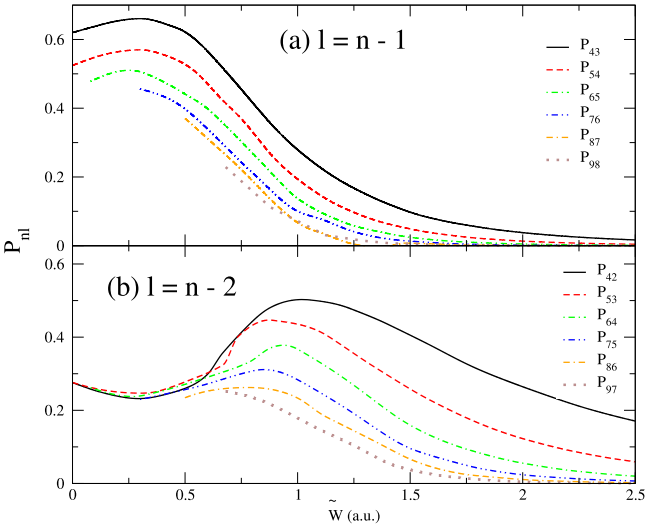

Figure 5. P_{nl} distributions, as a function of $\tilde{W}$, for (a) $l = n - 1$, and (b) $l = n - 2$. Lines, scaled nl-populations for different n shells, derived within the join CTMC-EI method considering charges $Z_P = 4 - 8$.

partial capture into the fundamental and first excited levels, i.e., $n = 1-4$. In this work the rule is extended to consider final levels in the range $n = 4-9$. In addition, we found that when the scaled cross sections S_n for the different levels are plotted together, all the CTMC-EI results can be gathered in a relatively narrow band, indicating a weak dependence on n of the universal function, i.e. $U_n(\tilde{W}) \simeq U(\tilde{W})$ for $4 \leqslant n \leqslant 9$, as shown in figure 2(a). In this figure we have split the $\tilde{W}$ range in two panels (upper and lower) in order to display clearly the different results.

Furthermore, we provide a simple expression to represent the approximate function $U(\tilde{W})$, which is valid for final levels with principal quantum numbers in the range $n = 4-9$. The proposed function (for σ_n expressed in cm^2) reads:

$$U\left(\tilde{W}\right) = \frac{a_1}{\left(b_1 + c_1\tilde{W}^2\right)^4} - \frac{a_2}{\left(b_2 + c_2\tilde{W}^2\right)^4}, \qquad (8)$$

where $a_1 = 3.46 \times 10^{-14}$ cm^2, $b_1 = 2.63$, $c_1 = 6.23$ (a.u.)$^{-2}$, $a_2 = 1.0 \times 10^{-16}$ cm^2, $b_2 = 2.21$, $c_2 = 1.43$ (a.u.)$^{-2}$. This function, also plotted in figure 2, is valid for positive $\tilde{W}$ values and can be used to evaluate capture from H(1s) to a

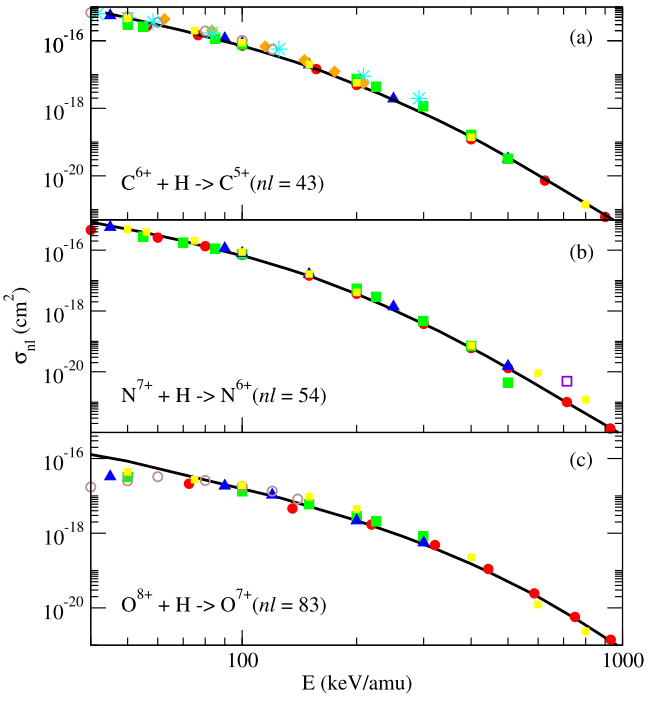

Figure 6. Partial CX cross sections σ_{nl} for: (a) $Z_P = 6$, $nl = 43$; (b) $Z_P = 7$, $nl = 54$; (c) $Z_P = 8$, $nl = 83$. Solid black line, present scaling; calculations: ● EIA, ■ CTMC, ▲ AOCC [35], ♦ CDW [39], ○ CTMC [40], ✳ FBA [34], □ CDW [43], ■ AOCC [41].

given n-shell through equation (7) considering velocities $v \gtrsim 2$ a.u., as well as lower energies (i.e. $E \gtrapprox 70$ keV/ amu) if the inequality $\tilde{z}_P > 1$ is satisfied. Notice that all the CTMC-EI results displayed in figure 2(a) (more than 500 S_n-values that cover an extended cross section range of almost 9 orders of magnitude) can be approximated by equation (8) with a maximum relative error of 40% at most, decreasing as the impact velocity augments.

Other theoretical methods also verify the universal behavior given by equation ((8), as shown in figure 2 (b), where scaled partial cross sections S_n, defined by equation (7), are plotted as a function of $\tilde{W}$ for different sets of theoretical data: those of Igenbergs *et al* [35] and Toshima and Tawara [41] obtained with the AOCC; those of Schultz *et al* [38] and Olson *et al* [40] obtained with the CTMC; those of Mandal *et al* [39] and Saha *et al* [43] obtained with the continuum distorted wave (CDW); and those of Belkić *et al* [34] obtained with the FBA. We observe that the different theoretical and experimental data lie again inside a narrow band around the universal curve of equation (8), assuring the validity of the proposed scaling. We have also included in figure 2 (b) results for C^{6+} projectiles and final capture levels $n = 4-8$ extracted from the ADAS website [42], considering the energy range $E \geqslant 70$ keV/amu. Differences between the recommended ADAS data for the intermediate and high energy regions and the ones derived from the universal curve were found lower than 15% and 10%, respectively. Notice that the scaling rule of equation (8) becomes specially useful for high $\tilde{W}$ values and highly excited n levels, where theoretical results are particularly scarce.

In order to illustrate the utility of the n-resolved scaling law, we compare in figure 3 partial cross sections for Ne^{10+} projectiles, available in the literature, with results derived from equations (7) and ((8)), considering final n levels close to the most populated one. Results of figure 3 confirm that the proposed scaling provides reasonable predictions for projectiles with $Z_P > 8$.

3.2. Scaling for nl-distributions

We investigate the nl-distributions, defined as $P_{nl} = \sigma_{nl}/\sigma_n$, with σ_{nl} the partial CX cross section into the nl subshell, which is obtained as $\sigma_{nl} = \sum_m \sigma_{nlm}$. Using equations (3) and (6) we derive the following scaling rule for P_{nl}:

$$P_{nl} = \frac{\sigma_{nl}}{\sigma_n} \simeq U_{nl}\left(\tilde{W}\right) \simeq \sum_m \frac{u_{nlm}\left(\tilde{W}\right)}{U_n\left(\tilde{W}\right)}, \qquad (9)$$

where U_{nl} is assumed as an universal function. In figure 4 we plot CTMC and EI results for the P_{nl} distributions corresponding to Be^{4+}, B^{5+}, C^{6+}, N^{7+}, and O^{8+} projectiles, as a function of $\tilde{W}$, considering final n levels from $n = 4$ to $n = 9$. While the CTMC method is used to obtain the nl-distributions for the lower values of $\tilde{W}$, i.e. $\tilde{W} \leqslant 1.5$ a.u., the EI approach is employed to describe the high energy region, which corresponds to $\tilde{W} \geqslant 2.0$ a.u. In all the cases, the P_{nl} values derived from the CTMC approach match with those obtained with the EI theory in the intermediate region, which corresponds to scaled transferred momenta $\tilde{W}$ in the range between 1.5 and 2.0 a.u. Therefore, it is possible to derive practically universal U_{nl} functions for the different nl- subshells, which can be used to estimate partial angular momentum distributions for ionic projectiles with larger nuclear charges than the ones considered here. To build these curves we have used the join CTMC-EI method, connecting the results of both theories at an impact velocity $v \approx 2.2$ a.u.

As a general tendency we found that for low $\tilde{W}$ values, in the range $\tilde{W} \lesssim 0.5$ a.u., the capture proceeds to the subshell with the highest orbital momentum, i.e. $l = n - 1$, but the l-value corresponding to the maximal contribution decreases as the scaled momentum $\tilde{W}$ augments, as shown in figure 5, where the P_{nl} distributions for the orbital quantum numbers $l = n - 1$ and $l = n - 2$ are displayed as a function of $\tilde{W}$. Even though all the curves for $l = n - 1$ (or $l = n - 2$) present similar shapes, the population of the nl-subshell also depends on the main quantum number n, since as n increases, the position of the maximum slightly shifts towards lower $\tilde{W}$ values and its relative contribution diminishes. This behavior is expected to hold also for higher Z_P charges.

With the aim of providing a more precise representation of the P_{nl} functions for the different nl-subshells, numerical values corresponding to the universal distributions obtained from the join CTMC-EI method are tabulated in tables 1–6 in the appendix. These tables can be easily used to compute a

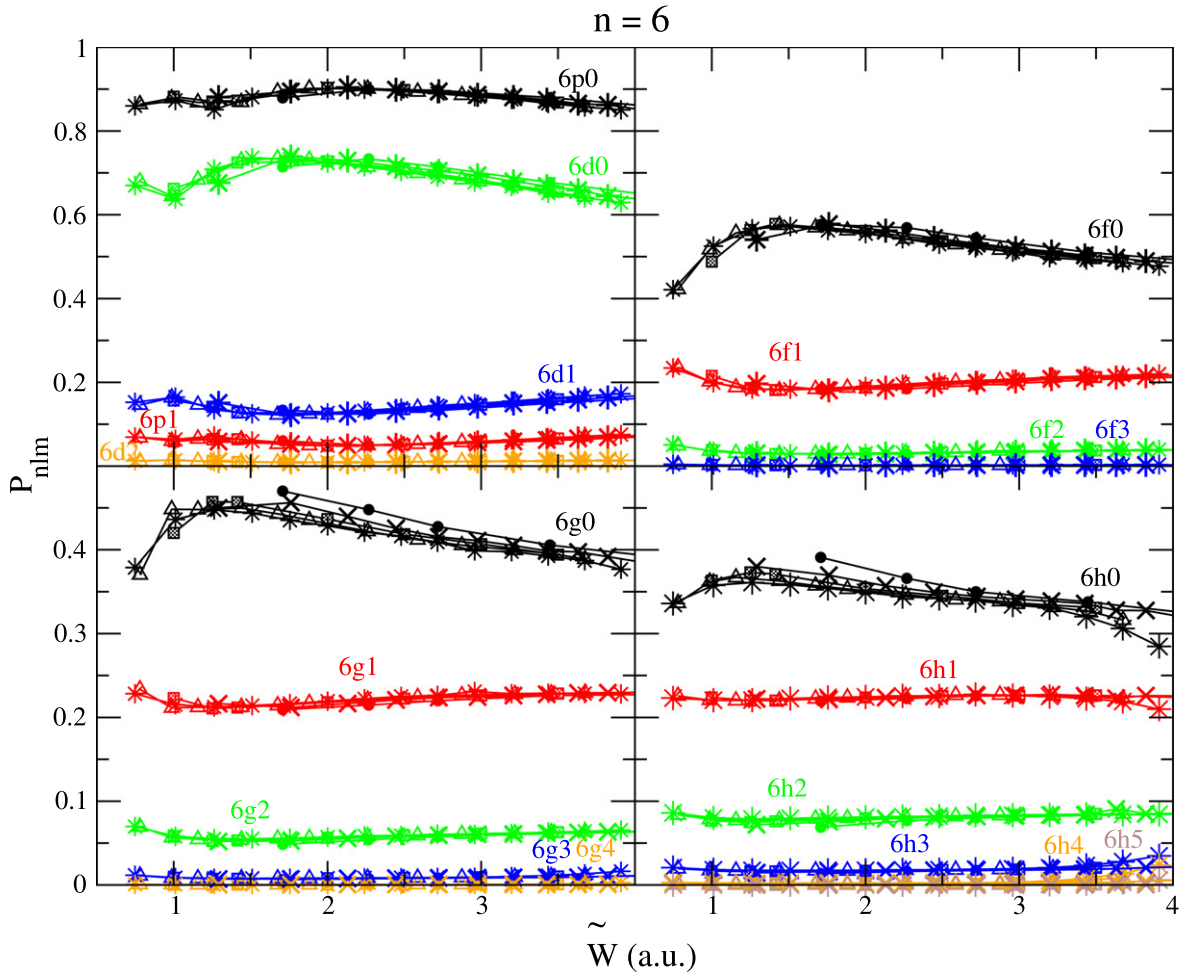

Figure 7. P_{nlm} distributions derived with the EI approach, for $n = 6$ as a function of $\tilde{W}$. Symbols: • Be^{4+}, x B^{5+}, □ C^{6+}, △ N^{7+}, * O^{8+}.

partial nl cross section for a given electronic transition and impact velocity. For example, σ_{43} for the $C^{6+} + H \rightarrow C^{5+}(nl = 43)$ process. First, we have to calculate σ_4 by applying equation (7) with $Z_P = 6$ and $\tilde{z}_P = 6/4$ as follows:

$$\sigma_4 = \left(\frac{6}{4}\right)^{-7} |C(6/v)|^2 U\left(\tilde{W}\right),$$

$$\text{with} \quad \tilde{W} = \frac{\tilde{v}^2 + (4/6)^2 - 1}{2\tilde{v}},$$

and $U(\tilde{W})$ from equation (8). Once we have computed σ_4, we only need to use equation (9) and table 1 to obtain σ_{43} as $\sigma_4 \times P_{43}$. As an illustrative example, in figure 6 we display partial CX cross sections, derived from the proposed scaling functions, as a function of the impact energy, considering: (a) $Z_P = 6$, $n = 4$, $l = 3$; (b) $Z_P = 7$, $n = 5$, $l = 4$; (c) $Z_P = 8$, $n = 8$, $l = 3$. These particular cases were only chosen as a proof of the efficacy of the proposed scaling rule. In all the cases, the scaling- derived curve, displayed with a black line, runs close to the CTMC and EI results, as well as to the theoretical data extracted from [35, 46]. Only for the O^{8+} example with $n = 8$, the scaling slightly overestimates the data for the lowest energies, since the condition $Z_P/n > 1$ is not verified.

3.3. Scaling for nlm-distributions

Finally, we study the scaling for the nlm-distributions, defined as $P_{nlm} = \sigma_{nlm}/\sigma_{nl}$, which are expected to verify:

$$P_{nlm} = \frac{\sigma_{nlm}}{\sigma_{nl}} \simeq U_{nlm}\left(\tilde{W}\right), \tag{10}$$

where U_{nlm} denotes again an universal function.

As an illustration, in figures 7 and 8 we plot the magnetic number distribution for the $n = 6$ and $n = 7$ shells, considering the quantization axis along the direction of the incidence velocity. In all the cases electrons are mainly captured to final states oriented parallel to the velocity, which correspond to $m = 0$, while the contribution of other final state orientations decreases as m increases. This is a general behavior, also observed for other n shells.

4. Conclusions

We have used two distinct approximations, CTMC and EI, in order to describe the CX process between multicharged ions and atomic hydrogen for a wide range of impact energies, encompassing from intermediate to high velocities. For five different bare projectiles, total and state-resolved CX

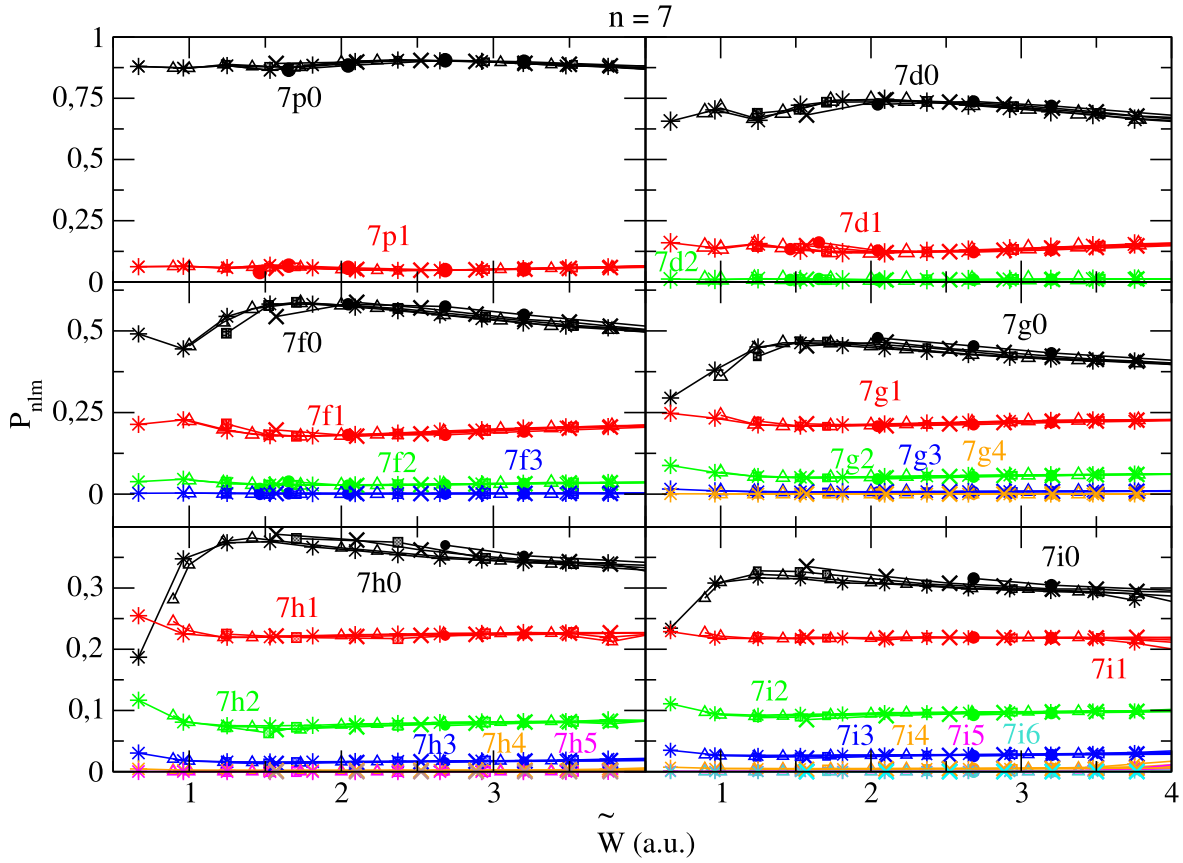

Figure 8. P_{nlm} distributions derived with the EI approach, for $n = 7$, as a function of $\tilde{W}$. Symbols: • Be^{4+}, x B^{5+}, ⊡ C^{6+}, △ N^{7+}, * O^{8+}.

cross sections derived with these methods show a good agreement with available experimental and theoretical data, being indicative of the accuracy of the considered descriptions. In addition, the fact that CTMC and EI state-selective cross sections for capture to highly excited levels, from $n = 4$ to $n = 9$, match between them in the intermediate energy region allowed us to extend previously derived scaling laws for shell and sub-shells capture distributions [13, 19] along the studied energy range. In the case of the *n*-resolved scaling, an analytical universal function in terms of the scaled transferred momentum $\tilde{W}$ is suggested, while for the *nl*-distributions, values obtained from the proposed scaling are listed in the appendix to facilitate their interpolation. These scaling rules are important tools, not only to display partial cross sections for different multicharged projectiles in a comprehensive way, but also to predict *n*-, *nl*-, and even *nlm*-distributions originated by highly charged ions.

Acknowledgments

M S G and J E M acknowledge financial support from CONICET, UBA, and ANPCyT of Argentina. A J and C I financial support from the projects ENE2011–28200 and ENE2014–52432-R of the Secretaría de Estado de Investigación, Desarrollo e Innovación (Spain).

Appendix A. Appendix: P_{nl} tables

Numerical values for the distribution corresponding to equation (9), derived from the proposed scaling rule, are listed in the following tables.

Table 1. $100 \times U_{nl}$ values for $n = 4$.

W_{P_z}	P_{40}	P_{41}	P_{42}	P_{43}
0.13	1	9	25	64
0.31	2	9	23	66
0.44	2	10	25	64
0.50	2	10	26	62
0.60	2	9	30	57
0.67	2	8	36	52
0.80	3	10	44	42
0.88	4	12	48	36
0.99	3	19	50	28
1.06	2	22	50	25
1.23	2	32	48	17
1.40	4	41	43	12
1.57	7	47	38	8
1.74	11	50	33	6
1.90	15	52	29	5
2.07	19	53	25	3
2.23	23	53	21	3
2.39	28	52	19	2
2.55	31	51	16	2
2.68	34	50	14	1

Table 2. $100 \times U_{nl}$ values for $n = 5$.

W_{P_z}	P_{50}	P_{51}	P_{52}	P_{53}	P_{54}
0.10	1	5	13	26	55
0.30	1	5	12	25	57
0.38	1	5	12	25	56
0.57	1	6	14	29	49
0.67	1	7	16	32	42
0.74	1	7	17	40	37
0.89	2	6	21	45	26
0.98	2	6	26	44	20
1.14	3	8	35	40	14
1.20	3	10	38	38	11
1.41	2	18	44	29	6
1.62	2	28	45	22	4
1.83	4	37	42	16	2
2.03	6	43	38	12	1
2.23	10	47	34	9	1
2.43	14	49	30	6	0
2.64	18	51	26	5	0
2.84	22	51	23	4	0
3.04	26	50	20	3	0
3.23	30	50	17	2	0

Table 3. $100 \times U_{nl}$ values for $n = 6$.

W_{P_z}	P_{60}	P_{61}	P_{62}	P_{63}	P_{64}	P_{65}
0.08	0	2	7	16	26	48
0.32	1	3	8	14	24	50
0.60	1	4	9	17	29	40
0.78	1	5	11	22	33	28
0.96	1	7	14	27	38	16
1.01	1	7	15	29	36	13
1.16	3	6	20	35	31	8
1.26	3	6	23	39	26	6
1.41	3	7	28	39	19	3
1.51	3	8	34	37	16	2
1.76	2	16	41	30	9	1
2.00	2	26	43	23	6	0
2.24	3	35	41	18	3	0
2.48	6	41	37	13	2	0
2.72	9	46	34	10	1	0
2.96	13	48	30	8	1	0
3.20	18	49	26	6	1	0
3.44	22	50	23	4	0	0
3.67	26	50	20	4	0	0
3.91	30	49	18	3	0	0

Table 4. $100 \times U_{nl}$ values for $n = 7$.

W_{P_z}	P_{70}	P_{71}	P_{72}	P_{73}	P_{74}	P_{75}	P_{76}
0.30	0	2	5	10	14	23	45
0.52	0	3	6	10	16	26	38
0.81	1	4	8	14	23	31	21
1.00	1	4	10	18	28	28	10
1.16	1	5	12	23	33	23	6
1.24	1	6	13	26	35	19	4
1.41	2	6	18	31	32	12	2
1.50	2	6	20	34	28	10	1
1.73	3	6	28	37	20	5	1

Table 4. (Continued.)

W_{P_z}	P_{70}	P_{71}	P_{72}	P_{73}	P_{74}	P_{75}	P_{76}
1.81	3	8	31	36	18	4	0
2.09	2	15	39	30	11	2	0
2.37	2	25	41	24	7	1	0
2.65	3	33	40	18	4	0	0
2.92	6	40	37	14	3	0	0
3.20	9	44	34	11	2	0	0
3.48	13	47	30	8	1	0	0
3.75	17	49	27	6	1	0	0
4.03	22	50	24	5	1	0	0
4.31	26	49	21	4	0	0	0
4.58	30	49	18	3	0	0	0

Table 5. $100 \times U_{nl}$ values for $n = 8$.

W_{P_z}	P_{80}	P_{81}	P_{82}	P_{83}	P_{84}	P_{85}	P_{86}	P_{87}
0.70	0	2	5	9	13	19	26	25
1.00	1	3	7	12	20	27	23	7
1.13	1	4	8	15	23	27	18	3
1.19	1	4	9	17	25	26	16	2
1.39	1	6	12	22	29	23	10	0
1.48	1	6	13	25	30	20	7	1
1.66	2	5	16	31	31	14	3	0
1.79	3	4	19	35	28	11	2	0
1.99	3	6	25	36	22	7	1	0
2.11	3	7	30	35	19	5	1	0
2.42	2	15	38	31	12	3	0	0
2.74	2	24	40	25	7	1	0	0
3.05	3	33	40	19	5	1	0	0
3.36	6	39	37	15	3	0	0	0
3.67	9	44	34	11	2	0	0	0
3.99	13	47	30	9	1	0	0	0
4.31	17	48	27	7	1	0	0	0
4.62	21	49	24	5	1	0	0	0
4.94	25	49	21	4	0	0	0	0
5.25	30	48	18	3	0	0	0	0

Table 6. $100 \times U_{nl}$ values for $n = 9$.

W_{P_z}	P_{90}	P_{91}	P_{92}	P_{93}	P_{94}	P_{95}	P_{96}	P_{97}	P_{98}
0.68	0	1	4	7	9	12	18	25	23
0.88	0	2	5	8	12	17	23	22	11
1.12	1	3	7	10	17	23	22	14	3
1.29	1	4	8	13	21	25	20	9	1
1.41	1	4	9	16	24	25	18	5	1
1.68	1	4	12	23	29	23	10	2	0
1.91	2	5	16	29	30	16	5	1	0
2.05	3	5	19	33	28	12	3	0	0
2.30	3	6	26	35	22	7	1	0	0
2.40	3	7	29	35	19	6	1	0	0
2.75	2	14	37	31	13	3	0	0	0
3.10	2	24	40	25	8	1	0	0	0
3.45	3	32	39	19	5	1	0	0	0
3.80	6	39	37	15	3	0	0	0	0
4.15	9	43	34	11	2	0	0	0	0
4.51	13	46	30	9	1	0	0	0	0
4.86	17	48	27	7	1	0	0	0	0
5.21	21	49	24	5	1	0	0	0	1
5.57	25	48	21	4	0	0	0	0	1

References

[1] Summers H P 1994 Need for cross sections in fusion plasma research *Cross Section Data* (*Advances in Atomic, Molecular, and Optical Physics* vol 33) ed M Inokuti (New York: Academic) pp 275–319
[2] Isler R C 1994 *Plasma Phys. Control. Fusion* **36** 171
[3] Thomas D M 2012 *Phys. Plasmas* **19** 056118
[4] Cravens T E 1997 *Geophys. Res. Lett.* **24** 105
[5] Cravens T E 2002 *Science* **296** 1042
[6] Otranto S, Olson R and Beiersdorfer P 2006 *Phys. Rev.* A **73** 022723
[7] Whyte D G, Isler R C, Wade M R, Schultz D R, Krstic P S, Hung C C and West W P 1998 *Phys. Plasmas* **5** 3694
[8] Beiersdorfer P, Bitter M, Marion M and Olson R 2005 *Phys. Rev.* A **72** 032725
[9] Otranto S, Olson R E and Beiersdorfer P 2007 *J. Phys. B: At. Mol. Opt. Phys.* **40** 1755
[10] Janev R K and Winter H 1985 *Phys. Rep.* **117** 265
[11] Smith R K, Foster A R and Brickhouse N S 2012 *Astron. Nachr.* **333** 301
[12] Fogle M, Wulf D, Morgan K, McCammon D, Seely D G, Draganić I N and Havener C C 2014 *Phys. Rev.* A **89** 042705
[13] Gravielle M S and Miraglia J E 1995 *Phys. Rev.* A **51** 2131–9
[14] Reinhold C O and Falcon C A 1988 *J. Phys. B: At. Mol. Opt. Phys.* **21** 2473
[15] Ryufuku H and Watanabe T 1979 *Phys. Rev.* A **19** 1538
[16] Cornelius K R, Wojtkowski K and Olson R E 2000 *J. Phys. B: At. Mol. Opt. Phys.* **33** 2017
[17] Foster A 2008 *PhD Thesis* University of Strathclyde
[18] Goffe T V, Shah M B and Gilbody H B 1979 *J. Phys. B: At. Mol. Phys.* **12** 3763
[19] Gravielle M S and Miraglia J E 1995 *Phys. Rev.* A **52** 851–4
[20] Janev R K 1983 *Phys. Scr.* **1983** 208
[21] Skinner C H 2009 *Phys. Scr.* **2009** 014022
[22] Doerner R, Baldwin M and Causey R 2005 *J. Nucl. Mater.* **342** 63–67
[23] Kallenbach A *et al* 2010 *Plasma Phys. Control. Fusion* **52** 055002
[24] Schweinzer J *et al* 2011 and the ASDEX Upgrade Team *Nucl. Fusion* **51** 113003
[25] Schwadron N A and Cravens T E 2000 *Astrophys. J.* **544** 558
[26] Otranto S and Olson R 2008 *Phys. Rev.* A **77** 022709
[27] Gravielle M S and Miraglia J E 1988 *Phys. Rev.* A **38** 5034–7
[28] Gravielle M S and Miraglia J E 1991 *Phys. Rev.* A **44** 7299–306
[29] Illescas C and Riera A 1999 *Phys. Rev.* A **60** 4546–60
[30] Jorge A, Errea L F, Illescas C and Méndez L 2014 *Eur. Phys. J.* D **68** 227
[31] Jorge A, Errea L F, Illescas C, Méndez L and Suárez J 2013 *Phys. Scr.* **2013** 014032
[32] Toshima N 1994 *Phys. Rev.* A **50** 3940–7
[33] Harel C, Jouin H and Pons B 1998 *At. Data. Nucl. Data Tables* **68** 279
[34] Belkić D, Saini S and Taylor H S 1987 *Phys. Rev.* A **36** 1601–17
[35] Igenbergs K, Schweinzer J, Veiter A, Perneczky L, Frühwirth E, Wallerberger M, Olson R E and Aumayr F 2012 *J. Phys. B: At. Mol. Opt. Phys.* **45** 065203
[36] Meyer F, Phaneuf R, Kim H, Hvelplund P and Stelson P 1979 *Phys. Rev.* A **19** 515–25
[37] Olson R E 1981 *Phys. Rev.* A **24** 1726–33
[38] Schultz D R, Krstić P S and Reinhold C O 1996 *Phys. Scr.* **1996** 69
[39] Mandal C R, Datta S and Mukherjee S C 1983 *Phys. Rev.* A **28** 1144–6
[40] Olson R E and Schultz D R 1989 *Phys. Scr.* **1989** 71
[41] Toshima N and Tawara H 1995 *Report NIFS-Data Series 26* National Institute for Fusion Science
[42] http://open.adas.ac.uk/
[43] Saha G C, Datta S and Mukherjee S C 1987 *Phys. Rev.* A **36** 1656–62
[44] Errea L F, Illescas C, Méndez L, Pons B, Riera A and Surez J 2004 *J. Phys. B: At. Mol. Opt. Phys.* **37** 4323
[45] Errea L F, Illescas C, Méndez L, Pons B, Riera A and Surez J 2006 *J. Phys. B: At. Mol. Opt. Phys.* **39** L91
[46] Igenbergs K 2011 Calculation of cross sections relevant for diagnostics of hot fusion plasmas *PhD Thesis* Vienna University of Technology